Assembly of Supramolecular Nanotubes from Molecular Triangles and 1,2-Dihalohydrocarbons

ARTICLE *in* JOURNAL OF THE AMERICAN CHEMICAL SOCIETY · OCTOBER 2014

Impact Factor: 12.11 · DOI: 10.1021/ja509480u

JACS
JOURNAL OF THE AMERICAN CHEMICAL SOCIETY

Article

pubs.acs.org/JACS

Assembly of Supramolecular Nanotubes from Molecular Triangles and 1,2-Dihalohydrocarbons

Zhichang Liu,[†] Guoliang Liu,[†,‡] Yilei Wu,[†] Dennis Cao,[†] Junling Sun,[†] Severin T. Schneebeli,[†] Majed S. Nassar,[§] Chad A. Mirkin,[†] and J. Fraser Stoddart*[,†]

[†]Department of Chemistry, Northwestern University, 2145 Sheridan Road, Evanston, Illinois 60208, United States

[§]Joint Center of Excellence in Integrated Nano-Systems (JCIN), King Abdul-Aziz City for Science and Technology (KACST), P.O. Box 6086, Riyadh 11442, Saudi Arabia

Supporting Information

ABSTRACT: Precise control of molecular assembly is a challenging goal facing supramolecular chemists. Herein, we report the highly specific assembly of a range of supramolecular nanotubes from the enantiomeric triangular naphthalenediimide-based macrocycles (*RRRRRR*)- and (*SSSSSS*)-NDI-Δ and a class of similar solvents, namely, the 1,2-dihalo-ethanes and -ethenes (DXEs). Three kinds of supramolecular nanotubes are formed from the columnar stacking of NDI-Δ units with a 60° mutual rotation angle as a result of cooperative [C−H···O] interactions, directing interactions of the [X···X]-bonded DXE chains inside the nanotubes and lateral [X···π] or [π···π] interactions. They include (i) semiflexible infinite nanotubes formed in the gel state from NDI-Δ and (*E*)-1,2-dichloroethene, (ii) rigid infinite nonhelical nanotubes produced in the solid state from NDI-Δ and $BrCH_2CH_2Br$, $ClCH_2CH_2Br$, and $ClCH_2CH_2I$, and (iii) a pair of rigid tetrameric, enantiomeric single-handed (*P*)- and (*M*)-helical nanotubes formed in the solid state from the corresponding (*RRRRRR*)- and (*SSSSSS*)-NDI-Δ with $ClCH_2CH_2Cl$. In case (i), only the electron-rich C═C double bond of (*E*)-1,2-dichloroethene facilitates the gelation of NDI-Δ. In cases (ii) and (iii), the lengths of *anti*-DXEs determine the translation of the chirality of NDI-Δ into the helicity of nanotubes. Only $ClCH_2CH_2Cl$ induces single-handed helicity into the nanotubes. The subtle interplay of noncovalent bonding interactions, resulting from the tiny structural variations involving the DXE guests, is responsible for the diverse and highly specific assembly of NDI-Δ. This research highlights the critical role that guests play in constructing assembled superstructures of hosts and offers a novel approach to creating supramolecular nanotubes.

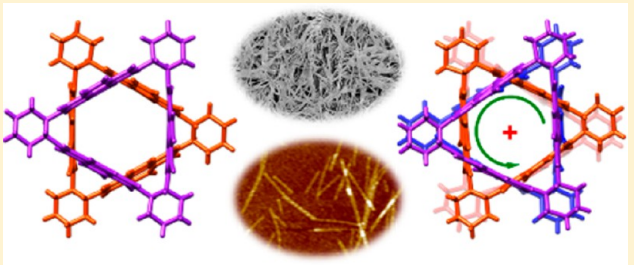

INTRODUCTION

In nature, tobacco mosaic virus (TMV)—one of the simplest of the viruses—exhibits a classical tubular architecture which is formed through the columnar stacking of double-layered protein disks with an RNA strand threading through the center of the assembly acting as the template.[1] Its superstructural stability results[2] from cooperative noncovalent bonding interactions between the proteins and the RNA nucleotides. Whether or not it is the apparent sheer simplicity of the virus that is responsible for its success, its tubular superstructure has helped turn it into a paradigm for the study of supramolecular assembly processes. A number of artificial supramolecular tubular assemblies have been designed[3] which mimic this class of natural superstructures with the goal of unraveling the mechanisms involved in the formation of such assemblies. These tubular assemblies display[4] promising applications in the fields of chemistry, biology, and materials science. Although taking advantage of cooperative hydrogen-bonding and/or π−π interactions to produce supramolecular nanotubes through coaxial stacking of macrocycles has been shown[4a,5] to occur spontaneously, creation of supramolecular nanotubes having a TMV-like superstructure from simple hosts with a threaded supramolecular chain as their template still remains a challenging goal which requires (i) the synergy generated by multiple noncovalent bonding interactions and (ii) a precise geometrical match between the hosts and guests lined up end-to-end, acting as templates. Guest-assisted host assembly has been demonstrated to play a critical role in crystal engineering[6] in the bottom-up construction of functional materials from a wide range of different building blocks. Weber and Vögtle[7] have described many examples relating to host−guest assembly in the solid state back in the 1970s. A classical hexameric "cyclamer" from six mutually hydrogen-bonded 1,3-cyclohexanedione molecules templated by benzene was featured in the literature in the 1980s by Etter,[8] while Braga[9] has employed organometallic sandwich compounds (e.g., cobaltocenium and ferrocene) as templates in more recent times to construct a series of noncovalent organic frameworks by means of charge-assisted [O−H···O] and [C−H···O] hydrogen bonds. Recently, we have demonstrated[10] that a pair of enantiomeric rigid triangular macrocycles, namely, (*RRRRRR*)- and (*SSSSSS*)-

Received: September 15, 2014

   dx.doi.org/10.1021/ja509480u | J. Am. Chem. Soc. XXXX, XXX, XXX−XXX

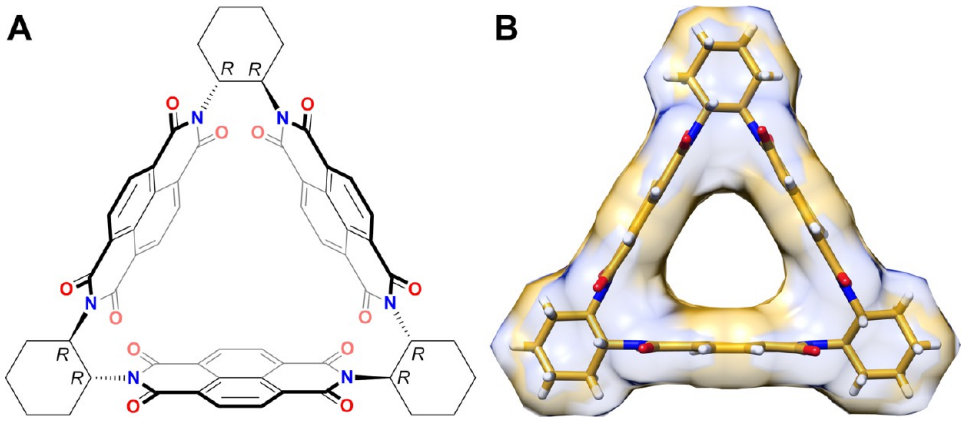

Figure 1. (A) Structural formula and (B) tubular representation superimposed upon a space-filling one of the solid-state structure of (*RRRRRR*)-NDI-Δ (*R*-Δ).

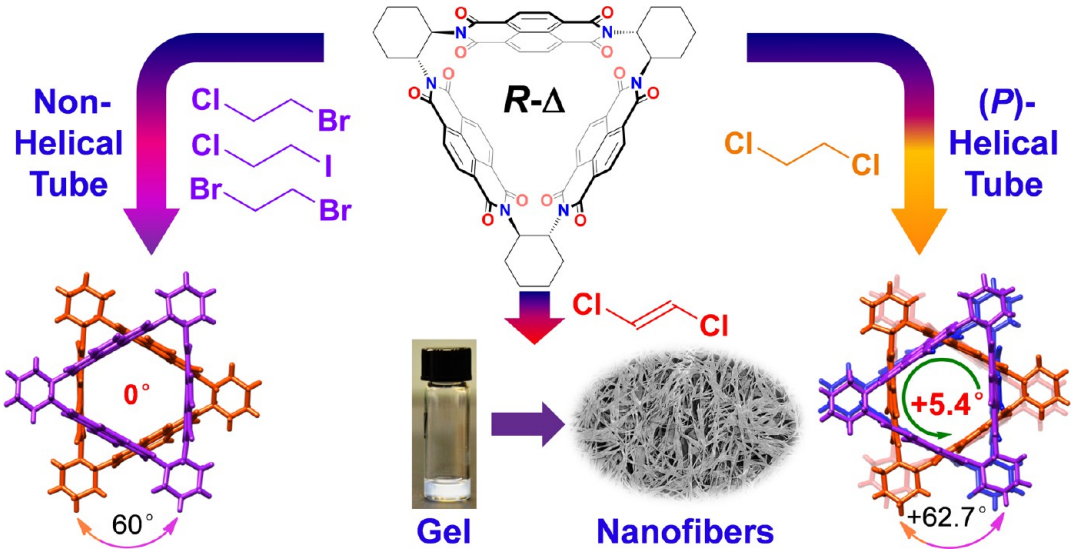

Figure 2. Schematic representation of three different assembly outcomes of *R*-Δ employing different DXE molecules. Middle: Gel specifically formed from *R*-Δ with (*E*)-DCE. Left: Nonhelical tubes formed from *R*-Δ with DBA, CBA, and CIA. Right: (*P*)-Helical tube specifically formed from *R*-Δ with DCA.

NDI-Δ (*R*-Δ and *S*-Δ in Figure 1), with tubular cavities are formed on joining up synthetically three naphthalenediimides (NDIs) with three (*RR*)- or (*SS*)-*trans*-1,2-cyclohexano units as linkers. Both *R*-Δ and *S*-Δ are able to assemble into their corresponding right- and left-handed [(*P*) and (*M*)] helices, respectively, through I_3^--induced $\pi-\pi$ stacking interactions with the NDI-Δ units, resulting in the formation of host–guest complexes [I_3^-⊂NDI-Δ] which propagate themselves in a helical fashion in the solid state when they crystallize. In essence, this assembly process displays the translation of the molecular chirality of the NDI-Δ units into the helicities of supramolecular assemblies. Although it was envisaged that these NDI-Δ units, free of the I_3^- template, could also become stacked in a columnar manner to produce supramolecular nanotubes, no evidence has been forthcoming thus far for the formation of this secondary superstructure either in solution or in the solid state. This lack of evidence implies that without additional directing noncovalent bonding interactions, the envisaged intermolecular [C–H···O] interactions[4j,11] between NDI-Δ units are not sufficient to hold them together to form tubular nanostructures. Hence, we have explored the possibility that [halogen···halogen] ([X···X]) interactions[12] provided by multiple guest molecules might cooperate with the weak [C–H···O] interactions in order to form host-based supramolecular nanotubes. On the basis of the lengths of 6.5 Å of the tubular channel of NDI-Δ and C···O distance ($d_{C\cdots O}$) of ∼3.2 Å of [C–H···O] hydrogen-bonding interactions, [X···X]-bonded 1,2-dihalo-ethane or -ethene (DXE) chains could be promising templates for the stacking of NDI-Δ in a coaxial manner to form nanotubes on account of the length of 4–5 Å of the *anti*-DXEs combined with 3–4 Å of [X···X] interactions. Here, we demonstrate the highly specific assembly of a diverse range of supramolecular nanotubes derived from NDI-Δ and a selection of DXEs. More notably, we demonstrate that NDI-Δ can be assembled to form (Figure 2) (i) an organogel which is made up of intertwining supramolecular nanotubes in a specific solvent, namely, (*E*)-1,2-dichloroethene ((*E*)-DCE), (ii) non-helical supramolecular nanotubes in the solid state under the influence of templating [X···X]-bonded $BrCH_2CH_2Br$ (DBA), $ClCH_2CH_2Br$ (CBA), or $ClCH_2CH_2I$ (CIA) supramolecular chains, and (iii) (*P*)- and (*M*)-helical supramolecular nanotubes in the solid state as a result of the columnar stacking of the *R*-Δ and *S*-Δ macrocycles, respectively, under the directing influence of [Cl···Cl]-bonded $ClCH_2CH_2Cl$ (DCA) supramolecular

dx.doi.org/10.1021/ja509480u | J. Am. Chem. Soc. XXXX, XXX, XXX–XXX

chains. We have combined (i) scanning electron (SEM) and atomic force (AFM) microscopies with (ii) X-ray crystallography, and (iii) NMR and CD spectroscopies to determine the superstructures and assembly mechanisms behind the formation of these secondary supramolecular nanotubes.

RESULTS AND DISCUSSION

Common halohydrocarbons, e.g., $CHCl_3$, CH_2Cl_2, CH_2Br_2, etc., are excellent solvents for *R*-Δ and *S*-Δ. Both enantiomerically pure *R*-Δ and *S*-Δ readily form single crystals on vapor diffusion of a poor solvent, such as MeOH or alkanes, into their solutions in halohydrocarbons. In a CH_2Cl_2/MeOH solvent system, both *R*-Δ and *S*-Δ crystallize[10] in the cubic space group $I2_13$ without exhibiting any $\pi-\pi$ stacking or coaxially hydrogen-bonding interactions between the NDI-Δ units. In a DBA/hexane solvent system in the presence of $[Bu_4N][I_3]$, both *R*-Δ and *S*-Δ crystallize[10] in the trigonal space group *R*3 as a result of $\pi-\pi$ stacking between adjacent $[I_3^-\subset$NDI-Δ$]$ building blocks, forming extended single-handed helical superstructures.

Gel Formation. Upon dissolving *R*-Δ in (*E*)-DCE with sonication, however, an organogel forms (Figure 2, middle) immediately. In order to check the general nature of this gelation phenomenon, a series of geometrical analogues of (*E*)-DCE, that is, (*Z*)-DCE, 1,2-dibromoethene [DBE, (*Z*/*E*) mixture], DCA, DBA, CBA, and CIA, was examined. Quite surprisingly, except for (*E*)-DCE, no gelation occurs in other DXEs, even in (*Z*)-DCE and DBE (*Z*/*E* mixture), an observation which indicates that only the electron-rich C═C double bond of (*E*)-DCE with its *anti* conformation can facilitate the gelation of *R*-Δ in a precise manner. It is noteworthy that the observation of supramolecular gelation, based on only rigid macrocycle gelators with solvents in the absence of additional guest cross-linkers, is quite rare.[13] Presumably, the (*E*)-DCE molecules play a dual role as both solvents and cross-linkers for the gelation of *R*-Δ. SEM of a freeze-dried xerogel sample reveals (Figure 3) that the gel is formed from intertwined nanoribbons (Figure 3A,B) which are further composed of fine nanofibers with diameters of tens of nanometers (Figure 3C). In order to gain insight into the mechanism behind the gelation of *R*-Δ, single-molecule AFM analyses were carried out to probe the molecular level details of this organogel. The AFM images of a sample prepared by spin-coating a fresh organogel onto a silicon wafer surface reveal several micrometer-long semiflexible nanofibers, in good agreement with the morphology of the xerogel observed by SEM. Since the determination of fiber width is significantly dependent on the size and shape of the AFM tip, height measurements were preferred in order to characterize the nanofiber cross sections. First of all, splitting and multistranded aggregation of fibers can be observed (Figure 4A,B) by AFM on individual nanofibers. The heights of the thicker parts were found (Figure 4B,C) to be almost twice or triple the height of the thinner nanofibers. These observations, taken together, strongly suggest that the thicker fibers originate from the aggregation of thinner fibers. More importantly, Figure 4D,E shows that numerous very fine discrete fibers of height 2.0 ± 0.4 nm (Figure 4F) with lengths of several hundreds of nanometers can also be observed. By performing a statistical analysis on an AFM image (Figure 4E), we were able to determine (Figure 4G) precisely the cross-section of these fine nanofibers. The most crowded nanofiber population has a height centered at ca. 2.0 nm; a dimension which corresponds remarkably well with the outer diameter of ca. 2.0 nm of the proposed supramolecular nanotube assembled (Figure 4H) from columnar stacking of *R*-Δ units with 60° rotation angle between neighboring units. This observation suggests that these fine fibers are supramolecular nanotubes formed at the single-molecule level in which the NDI-Δ units are stacked with 60° rotation angles in a columnar manner as a result of [C−H···O] interactions, in addition to the directing of the [Cl···Cl]-bonded (*E*)-DCE molecule chains in the center of the nanotubes.

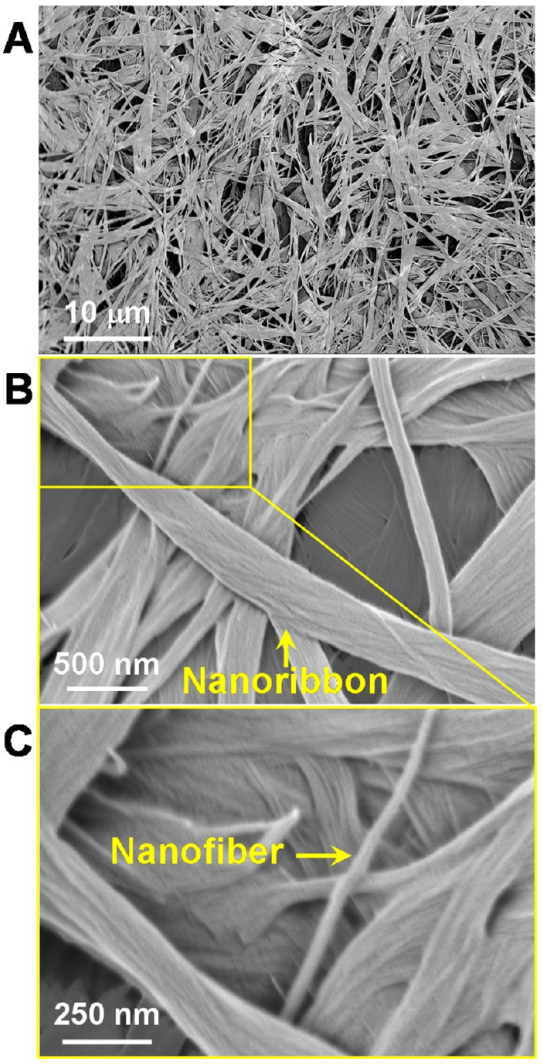

Figure 3. Morphologies of the xerogel sample of *R*-Δ with (*E*)-DCE by SEM (A) Large-scale network intertwined from nanoribbons. (B and C) Nanoribbons formed by the aggregation of small nanofibers.

X-ray Crystallography. Although SEM and AFM provided solid evidence for the mechanism of gelation of *R*-Δ in (*E*)-DCE, further atomic-level (super)structural evidence is essential to gain an understanding of the specificity of this gelation phenomenon. Since rapid gelation renders it difficult for NDI-Δ in (*E*)-DCE to crystallize, single-crystal X-ray (super)structures of NDI-Δ with other DXE molecules might be able to shine light on the reasons behind the difference in assembly behavior resulting from tiny variations in the constitutions of the solvent molecules. When the crystallization of *R*-Δ in DBA was attempted by slow vapor diffusion of hexane, we obtained single crystals suitable for X-ray crystallography. X-ray diffraction (XRD) analysis[14] reveals

dx.doi.org/10.1021/ja509480u | J. Am. Chem. Soc. XXXX, XXX, XXX−XXX

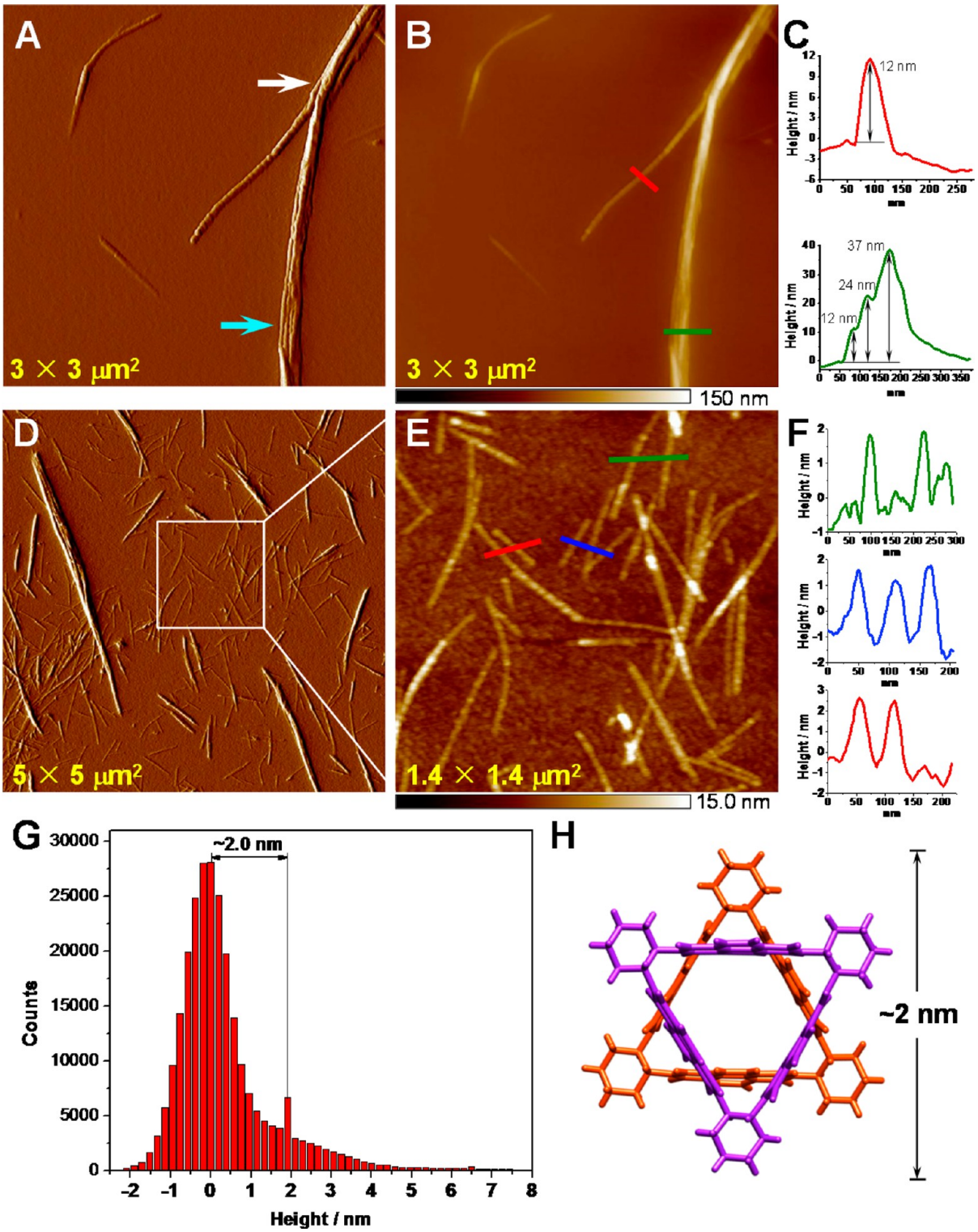

Figure 4. AFM images and morphological analyses of the gel. (A) The amplitude image of an area shows splitting (indicated by the white arrow) and multistranded aggregation (indicated by the blue arrow) of a large nanofiber. (B and C) The height image of the same area shows that the heights of the larger fibers are twice or triple the height of the smaller fiber which has split off from the larger one. The line colors in (B) correspond to the line colors in the profile plots (C). (D) The amplitude image of a selected area shows numerous fine nanofibers. (E and F) The zoomed-in height images of the area defined by the square in (D) show that the cross sections of most of these nanofibers have heights of around 2 nm. The line colors in (E) correspond to the line colors in (F). (G) A histogram displaying a statistical analysis of heights of (E). (H) A tubular representation of the top view of the columnar stacked *R*-Δ dimer with a 60° rotation angle between two *R*-Δ units having an outer diamater of ~2 nm.

(Figure 5) the formation of a 1:1 complex between *R*-Δ and DBA, namely, DBA⊂*R*-Δ, with an extended one-dimensional (1D) tubular secondary superstructure $[DBA]_n \subset [R\text{-}\Delta]_n$. The solid-state superstructure[14b] of DBA⊂*S*-Δ, obtained (Table S1) from *S*-Δ and DBA, is (Figure S1B) enantiomeric with that obtained for DBA⊂*R*-Δ. Inspection of the superstructure of

dx.doi.org/10.1021/ja509480u | J. Am. Chem. Soc. XXXX, XXX, XXX−XXX

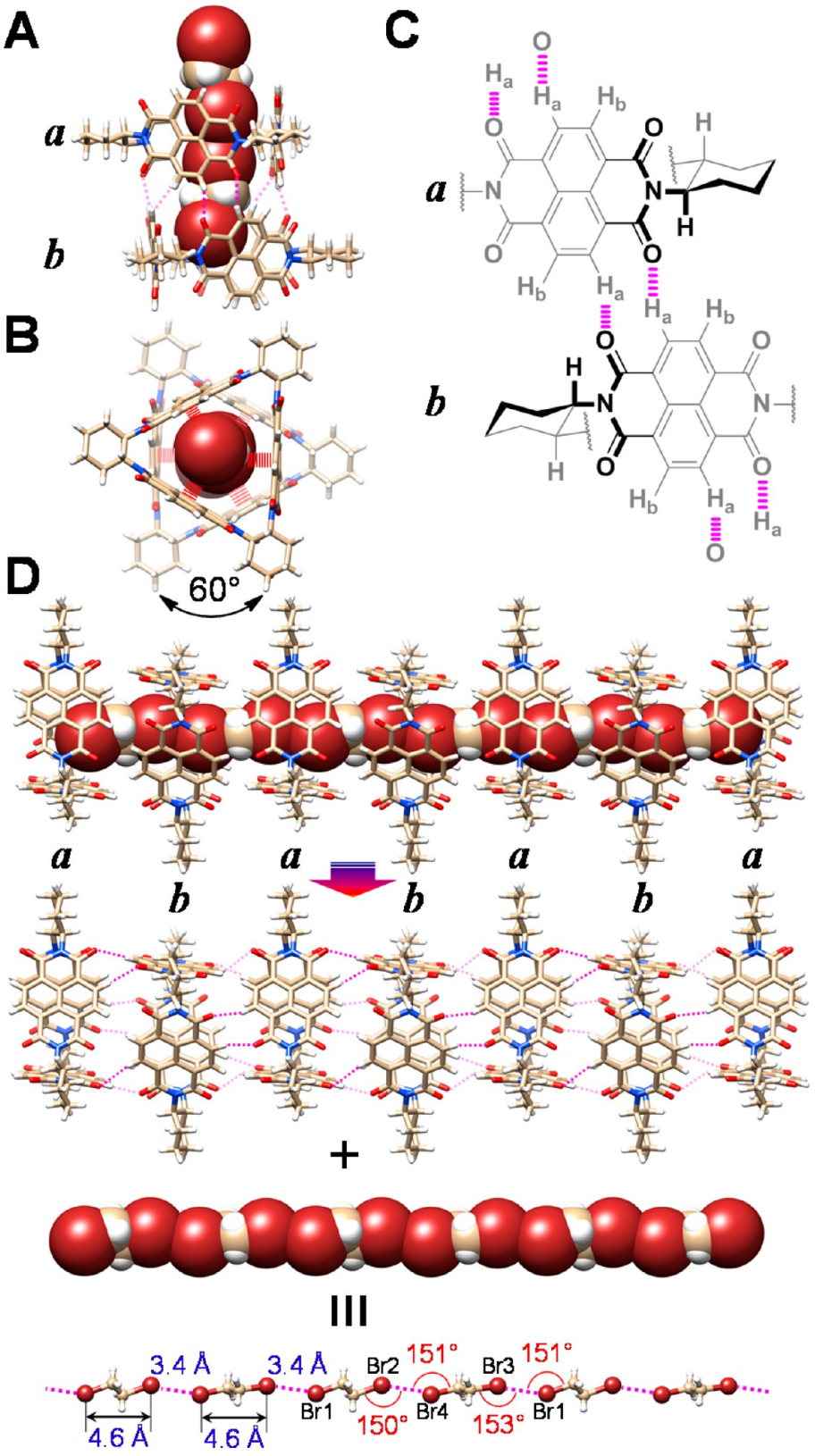

Figure 5. Single-crystal X-ray superstructure of DBA⊂*R*-Δ presented in tubular and space-filling formats. (A) Side-on view showing the relative orientation of two *R*-Δ *a* and *b*. (B) Top view showing that the coaxial DBA chain (space filling) is stabilized through latitudinal [Br···π] interaction (magenta hatched lines). (C) Schematic views of the [C−H···O] interactions (magenta hatched lines) between *R*-Δ units *a* and *b* as well as the ralative positions of the diastereotopic NDI protons H_a (*cis*) and H_b (*trans*) to the adjacent protons on the stereogenic center of the 1,2-cyclohexano moieties. (D) Schematic illustration of the one-dimensional superstructure in which the *R*-Δ tori form a continuous channel occupied by a [Br···Br]-bonded DBA chain. C, tan; H, white; O, red; N, blue; Br, brown. Hydrogen and halogen bonds are depicted as magenta hatched lines.

dx.doi.org/10.1021/ja509480u | *J. Am. Chem. Soc.* XXXX, XXX, XXX−XXX

DBA⊂*R*-Δ reveals (Figure 5A,C) that two *R*-Δ molecules *a* and *b* are stacked in a coaxial manner with a perpendicular rotation angle of 60° (a 3-fold screw axis) as a result of the stabilization by three pairs of self-complementary [C−H···O] interactions (mean $d_{C\cdots O}$ = 3.32 Å and mean $\theta_{C-H\cdots O}$ = 162°, Table S2) between the NDI units. By continuing to stack coaxially in this manner, these *R*-Δ *ab* pairs constitute an *abab*··· pattern which sustains a hexagonal channel (pore diameter ∼7.6 Å) in the direction of the stack. This channel is filled perfectly and stabilized by a coaxial "guest solvent wire", a [Br···Br]-bonded DBA chain, with latitudinal [Br···π] interactions (mean $d_{Br\cdots\pi}$ = 3.72 Å) (Figure 5B) between the Br atoms of the bridging DBA molecules and the NDI planes of *R*-Δ *ab* pairs. This DBA chain is composed (Figure 5D) of two kinds of DBA molecules which adopt *anti* conformations and are arranged in an alternating manner linked by longitudinal [Br···Br] bonding interactions. In these [Br···Br] contacts (Figure 5D), the two distances ($d_{Br\cdots Br}$ = 3.43 Å) are the same and significantly shorter than the sum (3.72 Å) of van der Waals radii of two Br atoms with the four angles $\theta_{C-Br\cdots Br}$ which range from 150 to 153°, averaging out at 151°. The relatively short $d_{Br\cdots Br}$ and the almost identical $\theta_{C-Br\cdots Br}$ of these [Br···Br] contacts are characteristic[15] of a well-defined Type-I [C−Br···Br−C] interaction. These discrete tubular superstructures pack (Figure S2) in parallel into a pseudo-rhombic fashion (α = 119°) in the *b*−*c* plane. Undoubtedly, this [Br···Br]-bonded DBA chain plays a critical role, similar to that of (*E*)-DCE, as a directing influence on the compact columnar stacking of the NDI-Δ units to form the tubular superstructure, a hypothesis which is supported by the observations that similar tubular superstructures are formed in the gel state of *R*-Δ in (*E*)-DCE, yet are not formed when monocarbon halohydrocarbons, such as $CHCl_3$, CH_2Cl_2, CH_2Br_2, etc. are employed during attempted crystallization.

In view of the formation of (*E*)-DCE- and DBA-directed tubular superstructures by both *R*-Δ and *S*-Δ, we decided to explore the assembly behavior of *R*-Δ and *S*-Δ with another DXE analogue, namely, DCA. A similar strategy was used during the crystallization[16] of the two complexes, namely, DCA⊂*R*-Δ and DCA⊂*S*-Δ, from *R*-Δ and *S*-Δ with DCA. In contrast to DBA⊂*R*-Δ and DBA⊂*S*-Δ, the enantiomeric solid-state superstructures of DCA⊂*R*-Δ and DCA⊂*S*-Δ exist (Table S1) in a different monoclinic space-group, i.e., *C*2. In comparison with the asymmetric unit of coaxially stacked NDI-Δ pair in DBA⊂*R*-Δ, the asymmetric unit in DCA⊂*R*-Δ is (Figure 6A) a tetrameric nanotube composed of four symmetry-inequivalent coaxially stacked *R*-Δ molecules *a*, *b*, *a*′, and *b*′ involving nine interfacial pairs of [C−H···O] interactions (mean $d_{C\cdots O}$ = 3.25 Å and $\theta_{C-H\cdots O}$ = 157°, Table S2) with pseudo-alternating orientations differing in having a counterclockwise rotation angle of +62.7°, rather than 60°. When viewed down (Figure 6A) the screw axis of the tetramer along, *R*-Δ *a* and *a*′ as well as *b* and *b*′ do not overlap completely but exhibit net counterclockwise rotation angles of +5.4° (2 × 62.7°−120°). In DCA⊂*S*-Δ, the clockwise rotation angle of −62.7° between adjacent *S*-Δ molecules and the net clockwise rotation angles of −5.4° between *S*-Δ *a* and *a*′ as well as *b* and *b*′ are observed (Figure 6B) in the enantiomeric complex. This observation highlights the fact that the corresponding (*P*)- and (*M*)-helical tetrameric nanotubes in DCA⊂*R*-Δ and DCA⊂*S*-Δ are achieved by induction of the molecular chiralities of *R*-Δ and *S*-Δ at the supramolecular level, respectively. The packing (Figure S3) of DCA⊂*R*-Δ and DCA⊂*S*-Δ reveals that both helicities are limited to the

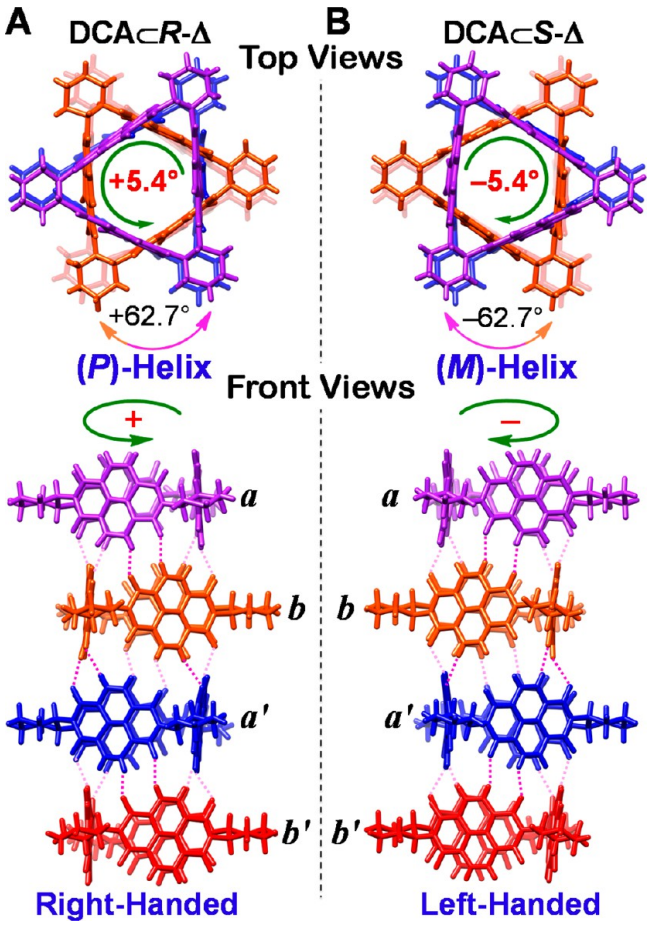

Figure 6. Single-crystal X-ray superstructures of DCA⊂*R*-Δ and DCA⊂*S*-Δ presented in tubular formats. Top and front views of (A) left-handed helical DCA⊂*R*-Δ and (B) right-handed helical DCA⊂*S*-Δ. The four nonequivalent NDI-Δ units are highlighted in purple, orange, blue, and red, respectively. Green arrows indicate the net rotation angles between the NDI-Δ units *a* and *a*′ as well as *b* and *b*′. Double-colored arrows show the relative rotation angle between the neighboring NDI-Δ units. Hydrogen bonds are depicted as magenta hatched lines.

tetrameric nanotubes, bundles of which are arranged in a zigzag pattern with an angle of 161° subtended between them. The breaking of long-range helicity is not unreasonable since, if the helicity was continuous, a complete helical pitch with a rotation angle of 60° would have to be composed of at least 12 tetramers with a length of ∼36 nm—an unacceptable dimension in crystal unit cells of small molecules—on account of the rotation angle of only 5.4° for each tetramer. Although the DCA molecules inside the nanotubes of DCA⊂*R*-Δ and DCA⊂*S*-Δ could not be refined satisfactorily, it is believed that these molecules play the same role as a director as do the DBA molecules in the formation of the tubular secondary superstructures on account of their similar molecular dimensions aided and abetted by [X···X] and [X···π] bonding interactions.

In order to shed light on the mechanism of the transfer of chirality from *R*-Δ and *S*-Δ into the supramolecular helicities, the tetramer (Figure 7A) in DCA⊂*R*-Δ is compared with its analogue—a tetrameric segment (Figure 7B) in the infinite tubular DBA⊂*R*-Δ. In contrast with the average 7.88 Å (respectively 7.90, 7.85, and 7.90 Å) of the centroid distance $d_{centroid\cdots centroid}$ between the *R*-Δ tori in DBA⊂*R*-Δ, the average $d_{centroid\cdots centroid}$ is 7.86 Å (respectively 7.87, 7.86, and 7.85 Å) in

dx.doi.org/10.1021/ja509480u | J. Am. Chem. Soc. XXXX, XXX, XXX−XXX

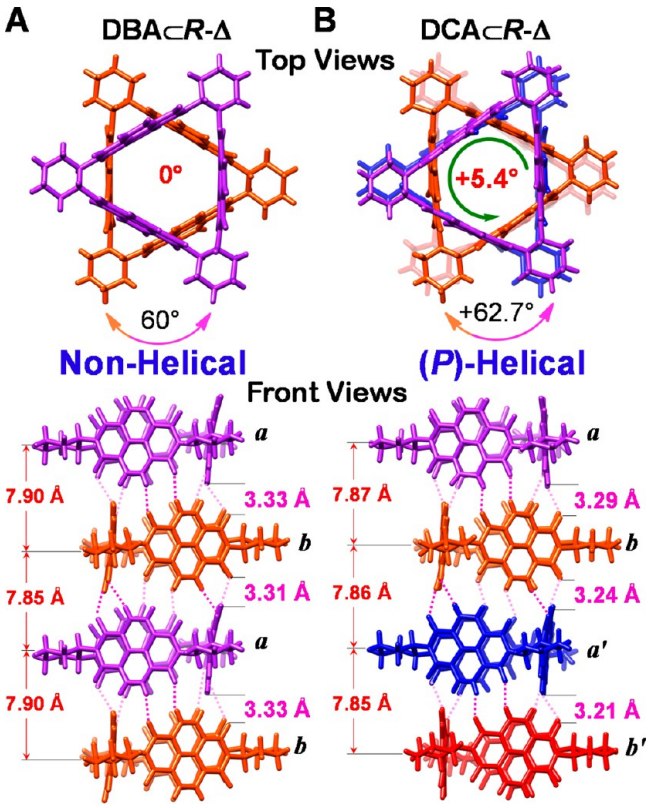

Figure 7. Comparison of single-crystal X-ray superstructures. (A) Nonhelical tetrameric unit of DBA⊂*R*-Δ. (B) (*P*)-Helical tetrameric DCA⊂*R*-Δ. Nonequivalent *R*-Δ units are highlighted with different colors. Green arrows indicate the net rotation angles between the NDI-Δ units *a* and *a*′ as well as *b* and *b*′. Double-colored arrows show the relative rotation angle between the neighboring NDI-Δ units. Hydrogen bonds are depicted as magenta hatched lines and mean $d_{C\cdots O}$ are present magenta color. DBA molecules inside the channel of DBA⊂*R*-Δ are omitted for the sake of clarity.

DCA⊂*R*-Δ. The mean [C−H···O] interaction distances $d_{C\cdots O}$ between three interfaces in DBA⊂*R*-Δ are (Table S2) 3.33, 3.31, and 3.33 Å (overall mean 3.32 Å), while the mean $d_{C\cdots O}$ in DCA⊂*R*-Δ are (Table S2) 3.29, 3.24, and 3.21 Å (overall mean 3.25 Å). The 0.07 Å shorter overall mean $d_{C\cdots O}$ of DCA⊂*R*-Δ implies that there are stronger hydrogen-bonding interactions between *R*-Δ in DCA⊂*R*-Δ which thus give rise to the 0.02 Å shorter of mean $d_{centroid\cdots centroid}$ between *R*-Δ. In addition, the 157° of mean $\theta_{C-H\cdots O}$ in DCA⊂*R*-Δ is 5° smaller than the 162° of mean $\theta_{C-H\cdots O}$ in DBA⊂*R*-Δ. The top views show (Figure 7B) clearly that, while the tetrameric nanotube in DBA⊂*R*-Δ is nonhelical, the one in DCA⊂*R*-Δ is (*P*)-helical with a net counterclockwise rotation angle of +5.4°. All these differences between the superstructures of DBA⊂*R*-Δ and DCA⊂*R*-Δ can be ascribed to the subtle differences between DBA and DCA. In DBA⊂*R*-Δ, the geometrical dimension of the [Br···Br]-bonded DBA chain is perfectly compatible with that of the columnar stacking superstructure, and each DBA molecule acts as a linker between two *R*-Δ units. In contrast, the length of 4.33 Å for the *anti*-conformation in DCA is (Figure S4) 0.29 Å shorter than that of 4.62 Å for *anti*-DBA. If DCA molecules form an infinite chain inside the consecutive nanotube, the lengths of the DCA chain and the NDI-Δ nanotube will become mismatched such that some DCA molecules will be unable to act as a linker of two NDI-Δ units. As a consequence, like a Vernier system,[17] the complex between the DCA chain and the NDI-Δ nanotube will inevitably be broken into nonconsecutive segments with a specific length, rationalizing the presence of the nonconsecutive tetrameric tubular complex in DCA⊂*R*-Δ. The disorder involving DCA can be ascribed to the oscillation along the channel direction that results from the mismatched lengths of the [Cl···Cl]-bonded trimeric DCA chain with the tetrameric NDI-Δ nanotube as well as the weaker [Cl···π] bonding interactions. Meanwhile, the shorter trimeric DCA chain also enforces the [C−H···O] interactions between three interfaces in the tetrameric nanotube as evidenced by the shorter mean $d_{C\cdots O}$. Consequently, the shorter $d_{C\cdots O}$ makes it possible for the asymmetric steric effect of the chiral *trans*-1,2-cyclohexylene groups to enforce in the twisted coaxial stacking of NDI-Δ that results in the formation of the single-handed helical supramolecular nanotubes.

In order to provide more evidence in support of the fact that the formation of the tetrameric helical nanotubes is determined by the shorter length of DCA, crystals of complexes between *R*-Δ, and two isologues of DBA and DCA—CBA and CIA—were grown and subjected to single-crystal XRD analysis. X-ray crystallography reveals (Table 1) that only DCA⊂*R*-Δ adopts a monoclinic space group (*C*2), while DBA⊂*R*-Δ and the other two complexes are isostructural since they crystallize in the same triclinic space group *P*1 with highly consistent unit cell parameters. On the basis of the same tubular superstructures of *R*-Δ being formed in DBA, CBA, and CIA, CBA and CIA are believed to play the same role as a director as do the DBA molecules by means of random [Cl···Cl], [Cl···Br], and [Br···Br] interactions for CBA and [Cl···Cl], [Cl···I], and [I···I] interactions for CIA in addition to [X···π] bonding interactions. Inspection of lengths of all four 1,2-dihaloethane molecules in their *anti*-conformations reveals that DCA (4.33 Å) has (Figure S4) the shortest length compared with CBA (4.48 Å), DBA (4.62 Å), and CIA (4.68 Å). This observation suggests that the length of guest molecule and the distance of [X···X] interaction indeed determine the formation of the single-handed helical host supramolecular nanotube and that DCA is the directing molecule with the most appropriate length. Isologues longer than DCA lead to longer [C−H···O] interactions which curtail the translation of molecular chirality of NDI-Δ into the supramolecular helicity, while the shorter monocarbon halohydrocarbons would most likely be too short to act as a

Table 1. Comparison of Unit Cell Parameters of Single Crystals[a] of *R*-Δ with Various 1,2-Dihaloethanes

	R-Δ			
parameter	DCA	DBA	CBA[b]	CIA[b]
crystal system	monoclinic	triclinic	triclinic	triclinic
space group	*C*2	*P*1	*P*1	*P*1
a, Å	46.28	15.75	15.66	15.76
b, Å	16.12	16.12	16.02	16.00
c, Å	40.43	16.21	16.14	16.15
α, °	90	119.44	119.67	119.38
β, °	90.03	100.23	99.40	98.61
γ, °	90	92.96	92.91	92.83

[a]All single crystals were grown by slow vapor diffusion of *n*-hexane into solutions of *R*-Δ in different 1,2-dihaloethanes at room temperature. [b]Both single-crystal structures obtained from *R*-Δ with CBA and CIA are isostructural with DBA⊂*R*-Δ and the solvent molecules inside the tubes could not be satisfactorily refined, and hence we report only the unit cell parameters.

dx.doi.org/10.1021/ja509480u | J. Am. Chem. Soc. XXXX, XXX, XXX−XXX

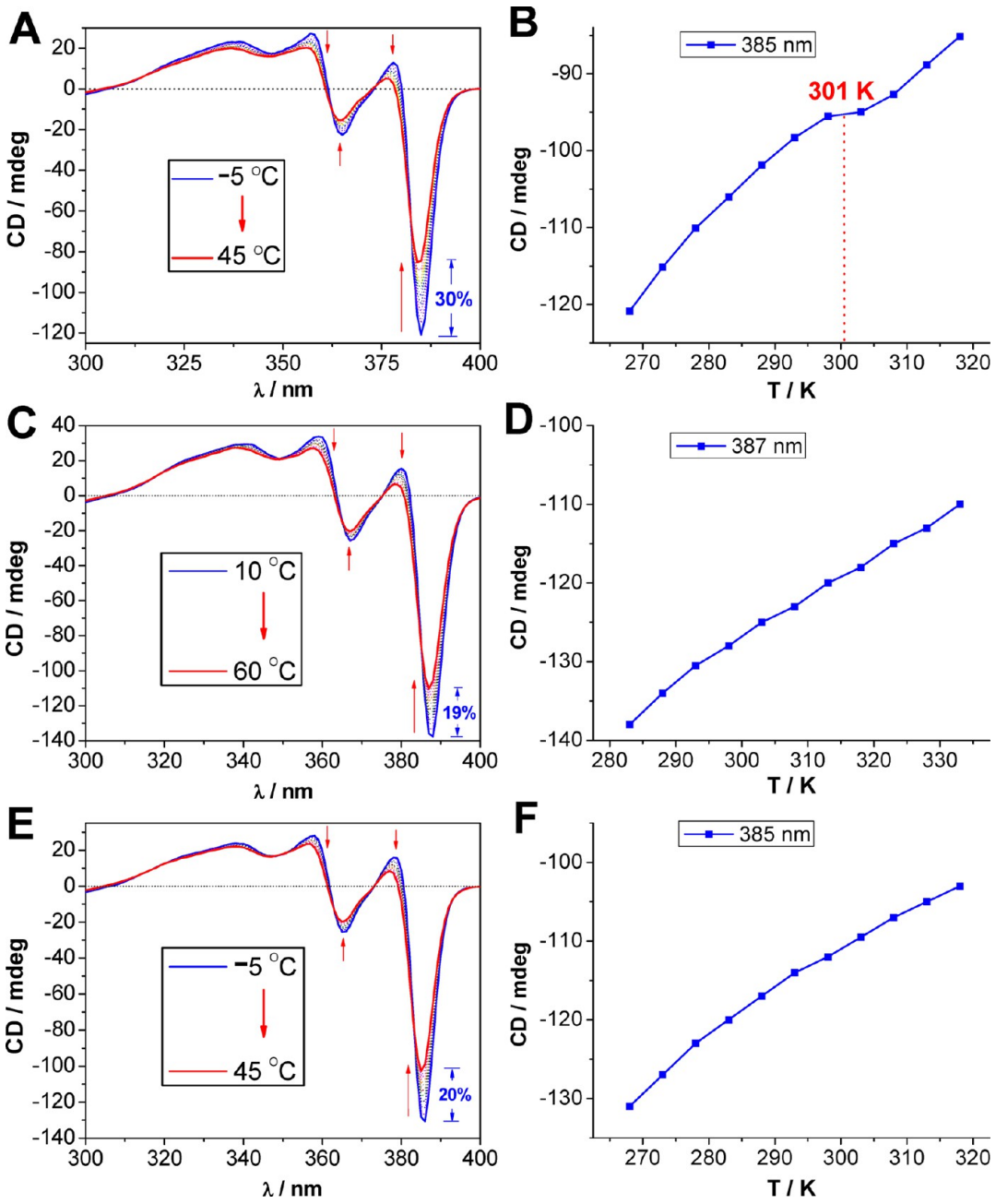

Figure 8. Temperature-dependent CD spectra of *R*-Δ in (A) (*E*)-DCE (1.21×10^{-4} M), (C) DBA (1.35×10^{-4} M) and (E) DCA (1.33×10^{-4} M). The plots (B), (D), and (F) record the dependence of the strongest CD signals in the corresponding CD spectra (A), (C), and (E) on temperature. Samples were kept for 10 min at the desired temperature before measurement. Temperature interval: 5 °C. Arrows indicate the directions of change in the CD intensities upon increasing the temperature of solutions.

linker between two NDI-Δ. It should be noted that this situation where molecular length determines translation of chirality of NDI-Δ can only be applied when the DXE molecules saturate the tubular structure. In the case of the gelation of *R*-Δ in (*E*)-DCE, the [$\pi\cdots\pi$] interaction between the inner NDI π-plane and the *anti* configuration associated with the C═C double bond replaces the [Cl$\cdots\pi$] interaction in order to support the tubular superstructure and thus restrict the axial movement of the (*E*)-DCE molecules. In order to form continuous tubular superstructures, the [Cl$\cdots$Cl] contact becomes longer and hence the weaker [Cl$\cdots$Cl] interactions will result in the flexibility of the 1D tubular superstructure that is in perfect agreement with the semiflexible morphology of the nanofibers observed by SEM and AFM. Meanwhile, the [$\pi\cdots\pi$] interaction between the outer NDI π-plane and the C═C double bond of (*E*)-DCE facilitates the aggregation of these semiflexible tubular superstructures to form intertwining networks which can then include solvents to form the final organogel.

Circular Dichroism Measurements. Temperature-dependent circular dichroism (CD) was carried out in order to probe the extent of aggregation in dilute (*E*)-DCE, DBA, and DCA solutions of the NDI-Δ molecules. Although the rigid chiral structure of nonaggregated *R*-Δ leads to a strong intrinsic Cotton effect on account of intramolecular exciton coupling between the three NDI units, upon heating a 1.21×10^{-4} M

dx.doi.org/10.1021/ja509480u | J. Am. Chem. Soc. XXXX, XXX, XXX−XXX

solution of *R*-Δ in (*E*)-DCE from −5 to +45 °C, the ellipticity of the CD spectra decreases (Figure 8A) by up to 30%. A plot (Figure 8B) of the CD intensity against temperature shows that the decrease in the Cotton effect is a two-step process with a transition point emerging at around 28 °C. These changes, which can be attributed to a reduction in the intermolecular exciton coupling between the *R*-Δ molecules, indicate that the *R*-Δ molecules are to some extent aggregated in (*E*)-DCE, even at low concentrations and undergo dissociation from one aggregation state to another at ca. +28 °C upon increasing the temperature of the solution. In contrast, upon increasing the temperatures of a 1.35×10^{-4} M solution of *R*-Δ in DBA from +10 to +60 °C and a 1.33×10^{-4} M solution of *R*-Δ in DCA from −5 to +45 °C, the Cotton effects observed in both CD spectra (Figure 8C,E, respectively) decrease in a linear fashion by 19% in DBA (Figure 8D) and by 20% in DCA (Figure 8F). These chiroptical characteristics imply that the aggregation behavior of *R*-Δ in both DBA and DCA is not dissimilar, yet quite different from that observed in (*E*)-DCE. This difference can be rationalized by the rapid onset of specific gelation of *R*-Δ molecules in (*E*)-DCE, a phenomenon which does not occur in DBA and DCA.

^{1}H NMR Spectroscopy. Thanks to the availability of deuterated DBA and DCA, we were able to probe the possible aggregation or inclusion properties of NDI-Δ in these solvents by ^{1}H and DOSY NMR spectroscopy. Variable-temperature (VT) ^{1}H NMR spectra (Figure S5) were recorded for *R*-Δ in $BrCD_2CD_2Br$ and $ClCD_2CD_2Cl$. At low temperatures, the diastereotopic NDI protons, designated as H_a and H_b in Figure 5C, resonate in both solvents as AB systems (Figure S5) with $\Delta\delta_{AB}$ values of 6.08 and 6.17 Hz, respectively, in deuterated DBA at +12 °C and DCA at −30 °C. Upon increasing the temperatures of the solutions of *R*-Δ, both in $BrCD_2CD_2Br$ (Figure S5A) and $ClCD_2CD_2Cl$ (Figure S5B), from 12 to 110 °C and from −30 to 80 °C, respectively, the resonances for both H_A and H_B experience substantial upfield shifts, but more so for H_A than for H_B, observations which might arise from the formation of the inclusion complexes between *R*-Δ with $BrCD_2CD_2Br$ and $ClCD_2CD_2Cl$. DOSY NMR spectroscopy was also carried out in order to detect if there is any intermolecular aggregation of *R*-Δ in solution. The diffusion coefficients (Figure S6) of *R*-Δ in $BrCD_2CD_2Br$ and $ClCD_2CD_2Cl$ are, respectively, 1.58×10^{-10} and 3.39×10^{-10} $m^2\ s^{-1}$, values which correspond to a hydrodynamic radius R_H of 0.69 nm that is comparable with the radius of ∼0.6 nm of *R*-Δ. We believe that significant aggregation of *R*-Δ in solution is not detectable by DOSY experiments because of the rapid dynamic exchange of species in solution.

CONCLUSIONS

In summary, from all three kinds of assembly of NDI-Δ in a class of special solvents, namely, 1,2-dihalo-ethanes and -ethenes (DXE), one common feature is demonstrated, i.e., that similar TMV-like tubular superstructures are formed from the columnar stacking of NDI-Δ units with a 60° rotation angle between neighboring triangles through cooperative [C−H···O] interactions and directed interactions of [X···X]-bonded DXE chains inside the nanotubes in addition to lateral [X···π] or [π···π] interactions. These tubular secondary superstructures can be divided into three categories: (i) semiflexible infinite supramolecular nanotubes in the gel state formed from NDI-Δ and unsaturated (*E*)-1,2-dichloroethene, (ii) rigid infinite nonhelical supramolecular nanotubes in the solid state, formed from NDI-Δ and the saturated 1,2-dihalo-alkanes $BrCH_2CH_2Br$, $ClCH_2CH_2Br$, and $ClCH_2CH_2I$, and (iii) a pair of rigid tetrameric, enantiomeric single-handed (*P*)- and (*M*)-helical supramolecular nanotubes in the solid state, generated upon crystallization of the corresponding *R*-Δ and *S*-Δ enantiomers with $ClCH_2CH_2Cl$. The subtle interplay of noncovalent bonding interactions, which result from tiny variations in the molecular geometries of the various guest solvents DXE, is responsible for the diverse and highly specific assembly of the same NDI-Δ host. This research highlights the critical role played by guests in the construction of assembled superstructures of hosts and offers a novel approach to the creation of tubular supramolecular assembles.

ASSOCIATED CONTENT

Supporting Information

Detailed information regarding the experimental methods and procedures, X-ray crystallographic data, and supportive figures and tables. This material is available free of charge via the Internet at http://pubs.acs.org.

AUTHOR INFORMATION

Corresponding Author

stoddart@northwestern.edu

Present Address

‡ Department of Chemistry, Virginia Tech, 900 West Campus Drive, Blacksburg, Virginia 24061, United States.

Notes

The authors declare no competing financial interest.

ACKNOWLEDGMENTS

We thank Amy A. Sarjeant and Charlotte L. Stern for carrying out the single-crystal XRD analyses. This research is part (Project 34-944) of the Joint Center of Excellence in Integrated Nano-Systems (JCIN) at King Abdulaziz City of Science and Technology (KACST) and Northwestern University (NU). The authors would like to thank both KACST and NU for their continued support of this research. C.A.M. acknowledges support from AFOSR under Award No. FA9550-12-1-0280. D.C. was supported by a NSF Graduate Research Fellowship; he also gratefully acknowledges support from a Ryan Fellowship awarded by the NU International Institute for Nanotechnology (IIN).

REFERENCES

(1) Klug, A. *Philos. Trans. R. Soc. London, Ser. B* **1999**, *354*, 531.
(2) Yang, Y.; Zhang, Y.; Wei, Z. *Adv. Mater.* **2013**, *25*, 6039.
(3) (a) Brunsveld, L.; Folmer, B. J. B.; Meijer, E. W.; Sijbesma, R. P. *Chem. Rev.* **2001**, *101*, 4071. (b) Shimizu, T.; Masuda, M.; Minamikawa, H. *Chem. Rev.* **2005**, *105*, 1401. (c) Casnati, A.; Liantonio, R.; Metrangolo, P.; Resnati, G.; Ungaro, R.; Ugozzoli, F. *Angew. Chem., Int. Ed.* **2006**, *45*, 1915. (d) Scanlon, S.; Aggeli, A. *Nano Today*, *3*, 22. (e) Liu, Z.-C.; Chen, C.-H.; Wang, H.-W.; Huang, Y.-C.; Kao, M.-J.; Lim, T.-S.; Luh, T.-Y. *Chem.—Asian J.* **2010**, *5*, 1425. (f) Gan, Q.; Ferrand, Y.; Bao, C.; Kauffmann, B.; Grélard, A.; Jiang, H.; Huc, I. *Science* **2011**, *331*, 1172.
(4) (a) Ghadiri, M. R.; Granja, J. R.; Milligan, R. A.; McRee, D. E.; Khazanovich, N. *Nature* **1993**, *366*, 324. (b) Nelson, J. C.; Saven, J. G.; Moore, J. S.; Wolynes, P. G. *Science* **1997**, *277*, 1793. (c) Orr, G. W.; Barbour, L. J.; Atwood, J. L. *Science* **1999**, *285*, 1049. (d) Cuccia, L. A.; Lehn, J.-M.; Homo, J.-C.; Schmutz, M. *Angew. Chem., Int. Ed.* **2000**, *39*, 233. (e) Fenniri, H.; Mathivanan, P.; Vidale, K. L.; Sherman, D. M.; Hallenga, K.; Wood, K. V.; Stowell, J. G. *J. Am. Chem. Soc.* **2001**, *123*, 3854. (f) Hecht, S.; Khan, A. *Angew. Chem., Int. Ed.* **2003**, *42*, 6021.

(g) Horne, W. S.; Stout, C. D.; Ghadiri, M. R. *J. Am. Chem. Soc.* **2003**, *125*, 9372. (h) Percec, V.; Dulcey, A. E.; Balagurusamy, V. S. K.; Miura, Y.; Smidrkal, J.; Peterca, M.; Nummelin, S.; Edlund, U.; Hudson, S. D.; Heiney, P. A.; Duan, H.; Magonov, S. N.; Vinogradov, S. A. *Nature* **2004**, *430*, 764. (i) Jin, W.; Fukushima, T.; Niki, M.; Kosaka, A.; Ishii, N.; Aida, T. *Proc. Natl. Acad. Sci. U.S.A.* **2005**, *102*, 10801. (j) Pantoş, G. D.; Pengo, P.; Sanders, J. K. M. *Angew. Chem., Int. Ed.* **2007**, *46*, 194. (k) Huang, Z.; Kang, S.-K.; Banno, M.; Yamaguchi, T.; Lee, D.; Seok, C.; Yashima, E.; Lee, M. *Science* **2012**, *337*, 1521. (l) Danial, M.; My-Nhi Tran, C.; Young, P. G.; Perrier, S.; Jolliffe, K. A. *Nat. Commun.* **2013**, *4*, 2780. (m) Gong, B.; Shao, Z. *Acc. Chem. Res.* **2013**, *46*, 2856. (n) Sato, K.; Itoh, Y.; Aida, T. *Chem. Sci.* **2014**, *5*, 136.

(5) (a) Venkataraman, D.; Lee, S.; Zhang, J.; Moore, J. S. *Nature* **1994**, *371*, 591. (b) Bong, D. T.; Clark, T. D.; Granja, J. R.; Ghadiri, M. R. *Angew. Chem., Int. Ed.* **2001**, *40*, 988. (c) Shimizu, L. S.; Hughes, A. D.; Smith, M. D.; Davis, M. J.; Zhang, B. P.; zur Loye, H.-C.; Shimizu, K. D. *J. Am. Chem. Soc.* **2003**, *125*, 14972. (d) Couet, J.; Biesalski, M. *Soft Matter* **2006**, *2*, 1005. (e) Iwanaga, T.; Nakamoto, R.; Yasutake, M.; Takemura, H.; Sako, K.; Shinmyozu, T. *Angew. Chem., Int. Ed.* **2006**, *45*, 3643. (f) Gong, H.-Y.; Rambo, B. M.; Karnas, E.; Lynch, V. M.; Sessler, J. L. *Nat. Chem.* **2010**, *2*, 406. (g) Liu, Z.; Frasconi, M.; Lei, J.; Brown, Z. J.; Zhu, Z.; Cao, D.; Iehl, J.; Liu, G.; Fahrenbach, A. C.; Botros, Y. Y.; Farha, O. K.; Hupp, J. T.; Mirkin, C. A.; Stoddart, J. F. *Nat. Commun.* **2013**, *4*, 1855.

(6) (a) Braga, D. *Chem. Commun.* **2003**, 2751. (b) Desiraju, G. R. *J. Am. Chem. Soc.* **2013**, *135*, 9952.

(7) (a) Weber, E.; Vögtle, F. *Chem. Ber.* **1976**, *109*, 1803. (b) Tuemmler, B.; Maass, G.; Weber, E.; Wehner, W.; Vögtle, F. *J. Am. Chem. Soc.* **1977**, *99*, 4683. (c) Vögtle, F.; Weber, E. *Angew. Chem., Int. Ed. Engl.* **1979**, *18*, 753. (d) Weber, E.; Vögtle, F. *Angew. Chem., Int. Ed. Engl.* **1980**, *19*, 1030.

(8) (a) Etter, M. C.; Urbanczyk-Lipkowska, Z.; Jahn, D. A. *J. Am. Chem. Soc.* **1986**, *108*, 5871. (b) Etter, M. C. *Acc. Chem. Res.* **1990**, *23*, 120.

(9) (a) Braga, D.; Angeloni, A.; Grepioni, F.; Tagliavini, E. *Chem. Commun.* **1997**, 1447. (b) Braga, D.; Angeloni, A.; Grepioni, F.; Tagliavini, E. *Organometallics* **1997**, *16*, 5478. (c) Braga, D.; Maini, L.; Polito, M.; Tagliavini, E.; Grepioni, F. *Coord. Chem. Rev.* **2003**, *246*, 53.

(10) Schneebeli, S. T.; Frasconi, M.; Liu, Z.; Wu, Y.; Gardner, D. M.; Strutt, N. L.; Cheng, C.; Carmieli, R.; Wasielewski, M. R.; Stoddart, J. F. *Angew. Chem., Int. Ed.* **2013**, *52*, 13100.

(11) (a) Thaimattam, R.; Xue, F.; Sarma, J. A. R. P.; Mak, T. C. W.; Desiraju, G. R. *J. Am. Chem. Soc.* **2001**, *123*, 4432. (b) Sureshan, K. M.; Gonnade, R. G.; Shashidhar, M. S.; Puranik, V. G.; Bhadbhade, M. M. *Chem. Commun.* **2001**, 881.

(12) (a) Pedireddi, V. R.; Reddy, D. S.; Goud, B. S.; Craig, D. C.; Rae, A. D.; Desiraju, G. R. *J. Chem. Soc., Perkin Trans. 2* **1994**, 2353. (b) Mukherjee, A.; Tothadi, S.; Desiraju, G. R. *Acc. Chem. Res.* **2014**, *47*, 2514.

(13) (a) Balakrishnan, K.; Datar, A.; Zhang, W.; Yang, X.; Naddo, T.; Huang, J.; Zuo, J.; Yen, M.; Moore, J. S.; Zang, L. *J. Am. Chem. Soc.* **2006**, *128*, 6576. (b) Ren, C.; Xu, S.; Xu, J.; Chen, H.; Zeng, H. *Org. Lett.* **2011**, *13*, 3840. (c) Chen, G.; Jiang, M. *Chem. Soc. Rev.* **2011**, *40*, 2254. (d) Zheng, B.; Wang, F.; Dong, S.; Huang, F. *Chem. Soc. Rev.* **2012**, *41*, 1621. (e) Guo, D.-S.; Liu, Y. *Chem. Soc. Rev.* **2012**, *41*, 5907. (f) Qi, Z.; Schalley, C. A. *Acc. Chem. Res.* **2014**, *47*, 2222.

(14) (a) Crystal data for DBA⊂*R*-Δ: triclinic, space group *P*1 (no. 1), a = 15.747(10), b = 16.119(13), c = 16.205(12) Å, α = 119.442(4), β = 100.225(3), γ = 92.957(4)°, V = 3478.6(5) Å^3, T = 100.0, Z = 2, μ(Cu Kα) = 4.683 mm^{-1}, 10617 reflections measured, 10617 unique which were used in all calculations. The final R_1 was 0.0968 ($I > 2\sigma(I)$) and wR_2 was 0.2928 (all data). (b) Crystal data for DBA⊂*S*-Δ: triclinic, space group *P*1 (no. 1), a = 15.734(6), b = 16.067(6), c = 16.186(6) Å, α = 119.550(16), β = 100.205(18), γ = 92.936(18)°, V = 3457.0(2) Å^3, T = 99.97, Z = 2, μ(Cu Kα) = 4.713 mm^{-1}, 13977 reflections measured, 13977 unique which were used in all calculations. The final R_1 was 0.0525 ($I > 2\sigma(I)$) and wR_2 was 0.1478 (all data). CCDC 1019483 (DBA⊂*R*-Δ) and 1019484 (DBA⊂*S*-Δ) contain the supplementary crystallographic data for this paper. These data can be obtained free of charge from The Cambridge Crystallographic Data Centre via www.ccdc.cam.ac.uk/data_request/cif.

(15) Desiraju, G. R.; Parthasarathy, R. *J. Am. Chem. Soc.* **1989**, *111*, 8725.

(16) (a) Crystal data for DCA⊂*R*-Δ: monoclinic, space group *C*2 (no. 5), a = 46.275(15), b = 16.117(5), c = 40.426(14) Å, β = 90.025(2)°, V = 30150.6(17) Å^3, Z = 16, T = 100.07, μ(Cu Kα) = 0.872 mm^{-1}, 66099 reflections measured, 26104 unique (R_{int} = 0.0384) which were used in all calculations. The final R_1 was 0.0651 ($I > 2\sigma(I)$) and wR_2 was 0.1923 (all data);. (b) Crystal data for DCA⊂*S*-Δ: monoclinic, space group *C*2 (no. 5), a = 46.893(8), b = 16.319(3), c = 40.708(7) Å, β = 90.657(12)°, V = 31150.0(9) Å^3, Z = 16, T = 240.0 K, μ(Cu Kα) = 0.519 mm^{-1}, 156519 reflections measured ($4.37 \leq 2\theta \leq 130.35$), 51762 unique ($R_{int}$ = 0.0594) which were used in all calculations. The final R_1 was 0.0523 ($I > 2\sigma(I)$) and wR_2 was 0.1440 (all data). CCDC 1019481 (DCA⊂*R*-Δ) and CCDC 1019482 (DCA⊂*S*-Δ) contain the supplementary crystallographic data for this paper. These data can be obtained free of charge from The Cambridge Crystallographic Data Centre via www.ccdc.cam.ac.uk/data_request/cif.

(17) O'Sullivan, M. C.; Sprafke, J. K.; Kondratuk, D. V.; Rinfray, C.; Claridge, T. D. W.; Saywell, A.; Blunt, M. O.; O'Shea, J. N.; Beton, P. H.; Malfois, M.; Anderson, H. L. *Nature* **2011**, *469*, 72.